NANO LETTERS

pubs.acs.org/NanoLett Letter

Exciton-Enabled Meta-Optics in Two-Dimensional Transition Metal Dichalcogenides

Zeng Wang,[†] Guanghui Yuan,[†] Ming Yang, Jianwei Chai, Qing Yang Steve Wu, Tao Wang, Matej Sebek, Dan Wang, Lei Wang, Shijie Wang, Dongzhi Chi, Giorgio Adamo, Cesare Soci, Handong Sun, Kun Huang,* and Jinghua Teng*

Cite This: *Nano Lett.* 2020, 20, 7964−7972 Read Online

ACCESS | Metrics & More | Article Recommendations | Supporting Information

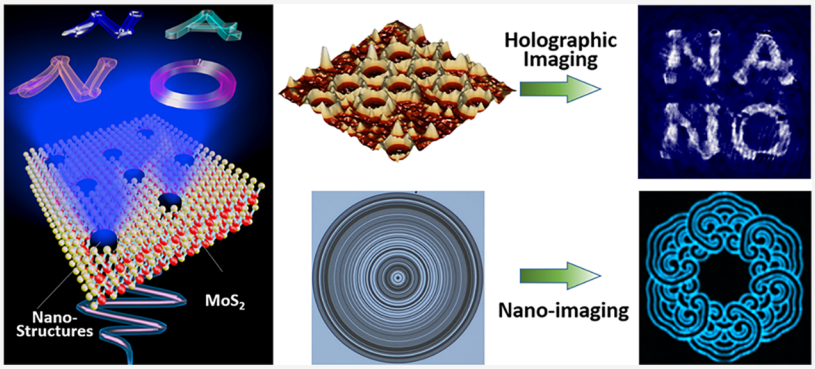

ABSTRACT: Optical wavefront engineering has been rapidly developing in fundamentals from phase accumulation in the optical path to the electromagnetic resonances of confined nanomodes in optical metasurfaces. However, the amplitude modulation of light has limited approaches that usually originate from the ohmic loss and absorptive dissipation of materials. Here, an atomically thin photon-sieve platform made of MoS_2 multilayers is demonstrated for high-quality optical nanodevices, assisted fundamentally by strong excitonic resonances at the band-nesting region of MoS_2. The atomic thin MoS_2 significantly facilitates high transmission of the sieved photons and high-fidelity nanofabrication. A proof-of-concept two-dimensional (2D) nanosieve hologram exhibits 10-fold enhanced efficiency compared with its non-2D counterparts. Furthermore, a supercritical 2D lens with its focal spot breaking diffraction limit is developed to exhibit experimentally far-field label-free aberrationless imaging with a resolution of ~0.44λ at λ = 450 nm in air. This transition-metal-dichalcogenide (TMDC) photonic platform opens new opportunities toward future 2D meta-optics and nanophotonics.

KEYWORDS: *exciton, transition-metal dichalcogenides, meta-optics, hologram, subdiffraction limit imaging, photonsieve*

INTRODUCTION

Optical elements modulate the phase and amplitude of light via tailoring the light−matter interaction in various applications. The underlying physics governing the light−matter interaction determines the performance of optical devices. Traditional refraction lenses and diffractive relief elements[1] employ the propagation phase that originates from the accumulated difference of optical path, which leads to a three-dimensional configuration with their thicknesses ranging from wavelengths to millimeters. Optical metasurfaces[2−7] realize the phase modulation with the electromagnetic resonances of well-confined nanomodes, resulting in a two-dimensional photonic platform with the subwavelength thickness and compact volume. By contrast, the amplitude modulation has limited physical origins such as the ohmic loss and absorptive dissipation[8] existing inherently in metal or plasmonic materials.

Recently, 2D material[9] optical devices[10−14] have been reported to shape light by patterning artificial micro/nanostructures. Compared with traditional optical metasurfaces, these 2D material meta-optics are promising for developing ultracompact optoelectronic components. Unfortunately, these 2D material meta-devices are still exploiting the traditional dielectric properties of 2D materials so that the exhibited performance is incomparable with traditional metasurface optics. Moreover, some devices made of hexagonal boron nitride (hBN)[15] and graphene oxide[16] have the

Received: July 2, 2020
Revised: October 9, 2020
Published: October 15, 2020

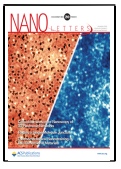

https://dx.doi.org/10.1021/acs.nanolett.0c02712
Nano Lett. 2020, 20, 7964−7972

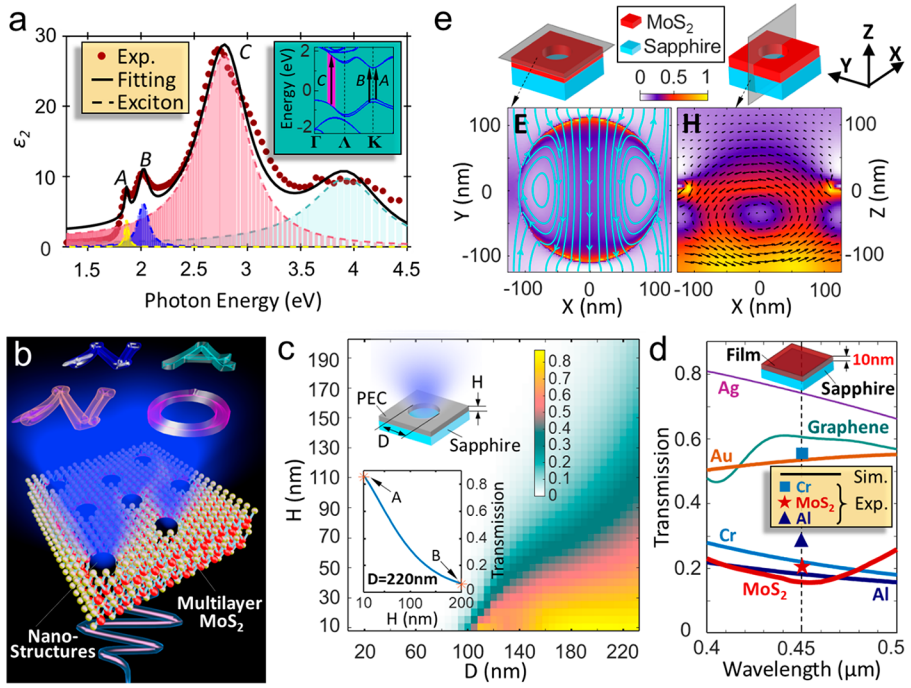

Figure 1. Working principle of MoS_2-based meta-optics. (a) Imaginary part (ε_2) of the relative permittivity of a multilayer MoS_2. The experimental permittivity is derived from the measured complex refractive index.[33] The Lorentz line shapes[49] are used to fit the experimental permittivity, thereby unveiling the contribution of A (yellow-dashed), B (blue-dashed), and C (pink-dashed) excitons to the imaginary part of permittivity. The C exciton dominates the absorption of light in a multilayer MoS_2 film because of the parallel valence and conduction bands (the purple region in the inset that displays the band structures of a monolayer MoS_2). (b) Sketch of shaping light with nanostructured multilayer MoS_2. (c) Transmission of light passing through a hole (with its diameter of D) in a PEC film with the thickness of H at the wavelength of 450 nm. The physical picture is sketched in the upper insert. The lower inset shows the optical transmission from a 220 nm diameter hole in a film with its thickness varying 5 to 200 nm. In two representative locations of A (H = 10 nm) and B (H = 200 nm), their transmissions are ~86% and ~6% respectively. (d) Optical transmission spectrum through a 10 nm thickness film made of Ag, Au, Cr, graphene, and MoS_2. The sapphire substrate is chosen to facilitate the preparation of good MoS_2 film due to its crystalline property. One can find that the MoS_2 film shows the most efficient blocking of light at the wavelengths of 400−480 nm. At the 450 nm wavelength of interest, a 10 nm thick MoS_2 film (star, ~22%) has much lower experimental transmission than a 10 nm thick Cr film (square, ~55%[37]). (e) Simulated electric (left panel) and magnetic (right panel) fields of a y-polarized 450 nm wavelength light passing through a 220 nm diameter hole that is made in a 10 nm thick MoS_2 film. The electric field at the top surface of the hole indicates a strong y-orientated dipole-like (as confirmed by its magnetic field at the x−z plane) intensity within the hole, but the intensity outside the hole is weak, which confirms the MoS_2 film as an efficient opaque screen.

thickness of 245 nm (~0.54λ) and 200 nm (~0.45λ), respectively, which are far beyond the phrase of 2D in optics. By using graphene,[10] MoS_2,[11] $PtSe_2$,[12] and $Sb2Te_3$,[13] the reported devices have thicknesses from a few to tens of nanometers and low efficiency (below 10.1%) caused by the insufficient optical modulation. Benefiting from strong local scattering of nanoparticles generated by femtosecond laser writing, a monolayer WSe_2 lens realizes the complex-amplitude modulation for diffraction-limited focusing and image.[14]

In contrast to the giant nonlinearity[17,18] of monolayer TMDCs, multilayer TMDCs support excitonic resonances that enable strong absorption even in few-nanometer thickness.[19−21] Although multilayer WS_2 microdisks have been reported recently as Mie resonators by utilizing the high-permittivity feature,[22] the resonating loss at visible frequencies is too high for optical phase-type nanodevices. Nevertheless, the strong-absorption feature makes multilayer TMDCs as the nearly perfect light-blockers for amplitude modulation. For example, photon sieves, composed of etched micro/nanostructures through an opaque film, have shown their merits in lens,[23−25] holograms,[26,27] orbital-angular-momentum manipulation,[28,29] and optical nanometrology.[30] These metal-based photon sieves demand the film thickness of hundreds of nanometers for blocking the undesired background efficiently. However, the thick film increases the coupling loss of waveguide modes,[31] thereby reducing optical transmission. Consequently, all reported photon sieves suffer from the low efficiency of several percentages.

Here, we utilize MoS_2 multilayers with strong exciton absorption governed by band-nesting effects to demonstrate high-performance meta-optics. Designed at the C exciton resonances, a MoS_2 photon-sieve hologram is demonstrated experimentally with a 10-fold enhanced efficiency compared with the non-2D photon-sieves; meanwhile, a proposed supercritical lens has exhibited the subdiffraction-limit nanofocusing and nanoimaging.

DESIGN PRINCIPLE

The MoS_2 is exemplified for the proof-of-concept demonstration of 2D TMDC meta-optics. For the TMDCs, the imaginary part (ε_2) of the relative permittivity is responsible for the absorption of light. Using the dipole approximation in quantum theory,[32] one has $\varepsilon_2(\omega) \approx 4\pi^2 e^2/(m^2\omega^2) \sum_{v,c} |d_{vc}|^2 \rho_{vc}(\omega)$[19] where e and m are the electric charge and the mass of electron, ω is the frequency of light, d_{vc} is the matrix element of dipole, and v and c label the states at the valence and conduction bands, respectively. The joint density of states $\rho_{vc}(\omega) \propto \int \frac{dS}{|\nabla_k (E_c - E_v)|}$, where the integral is calculated over the

https://dx.doi.org/10.1021/acs.nanolett.0c02712
Nano Lett. 2020, 20, 7964−7972

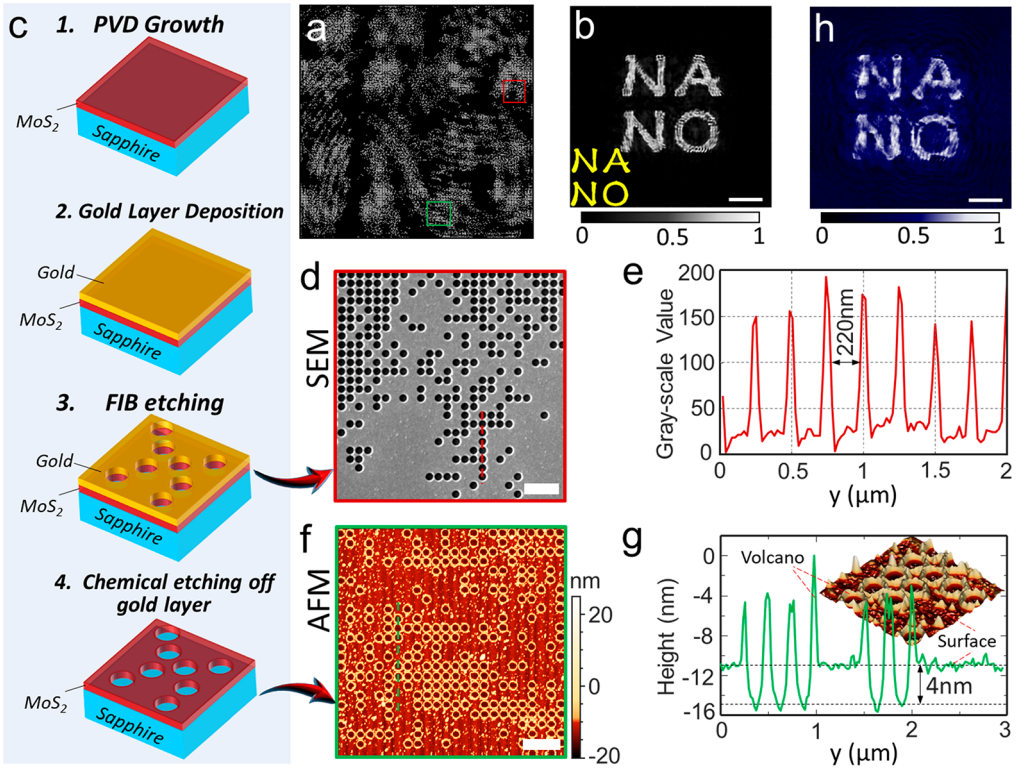

Figure 2. MoS_2-based photon nanosieve holograms. (a) Designed hologram with the 220 nm diameter holes in a pixel pitch of 250 nm × 250 nm. The total size of this hologram is 60 μm × 60 μm. (b) Simulated holographic image at the target plane of z = 200 μm. The inset shows the pattern of ideal image. Scale bar: 20 μm. (c) Fabrication procedures of MoS_2 photon nanosieve. (d) SEM image of the fabricated sample with the top gold layer. The imaging area corresponds to the location encircled within the blue square in b. Scale bar: 1 μm. (e) Gray scale value of SEM image along the red-dashed line in d for determining the diameter of holes. (f) AFM image of final pure-MoS_2 sample. The image is located within the green square in b. Scale bar: 1 μm. (g) Height profile extracted along the green-dashed line in f. Three-dimensional view of AFM image in the inset unveils that the volcano-like shapes (the height of ~6 nm) outside the etched holes arise because of the ion implantation[50] during the focused-ion-beam process. (h) Measured holographic image at the target plane of z = 200 μm.

entire two-dimensional Brillouin zone, $S(E)$ is a function of $E = E_c - E_v$, E_c, and E_v are the energies of states at the conduction and valence bands. Few-layer MoS_2 has three absorption bands corresponding to the A, B, and C excitons from low to high photon energy.[19,21] At the C exciton region, the parallel structures (named as band nesting[19]) of valence and conductor bands offer a nearly constant E so that $|\nabla_k(E)|$ approaches 0, yielding the divergent singularity in ρ_{vc}. It results in a significant increment of ε_2 (Figure 1a), hereby enhancing the absorption at the C exciton resonating wavelengths. Experimentally, high absorption close to 80% is confirmed from the measured absorption spectrum of 15-layer (~10 nm thickness) MoS_2 film grown by physical vapor deposition, where the maximum absorption is located at λ = 450 nm (Figure S1).

The 2D photon nanosieves (Figure 1b) have the nanoholes etched through a multilayer MoS_2 film. High-quality photon sieves demand high transmission through the holes (increase the efficiency) and strong absorption at the film region (reduce the undesired background). First, we investigate the optical transmission through the nanoholes milled in a perfect-electric-conductor film, which is chosen to calculate the pure transmission through only the holes and exclude the background that arises in an ultrathin film of realistic material. The simulation is done by using finite-difference time-domain (FDTD) method in a pixel pitch of 250 nm × 250 nm through setting the periodic boundaries in x/y directions and the perfect-matching layers in z direction (Figure S2). Our simulated results (Figure 1c) indicate that the large-diameter holes in a thinner film lead to high transmission. For example, a 220 nm diameter hole in a 10 nm thick film has the transmission of ~86% (A in the inset of Figure 1c), enhancing ~14 times compared with the ~6% transmission of a 200 nm thickness film (B in the inset of Figure 1c). Predicted by the coupled-mode theory,[23,31] the coupling length between the eigenmodes within the hole is shorter for a thinner film. Correspondingly, the coupling loss of every eigenmode is small, thus enhancing the transmission.

To balance high transmission of holes and strong absorption of films, we employ a 10 nm thick film here and compare the light-blocking validity between MoS_2 and other opaque materials. By using the experimental permittivity of MoS_2,[33] the simulated transmittance (Figure 1d) confirms that the multilayer MoS_2 offers a better blocking of light from 400 to 470 nm than silver, graphene, and gold.[34,35] Although aluminum (Al) and chromium (Cr) could be potential candidates to block the 450 nm wavelength light theoretically, it is extremely challenging to have a smooth 10 nm thick Al or Cr film, due to the large grain size of >20 nm. Consequently, the well-prepared Al and Cr films with 10 nm thickness were reported to have the experimental transmission of ~27%[36] and ~55%,[37] respectively, which lead to more background than ~20% of MoS_2 for photon nanosieves. Note that the multilayer MoS_2 is anisotropic, leading to both in-plane and out-of-plane components in its dielectric tensor.[22] Because of the difficulty in exciting the vertical dipole for multilayer MoS_2, the out-of-

https://dx.doi.org/10.1021/acs.nanolett.0c02712
Nano Lett. 2020, 20, 7964−7972

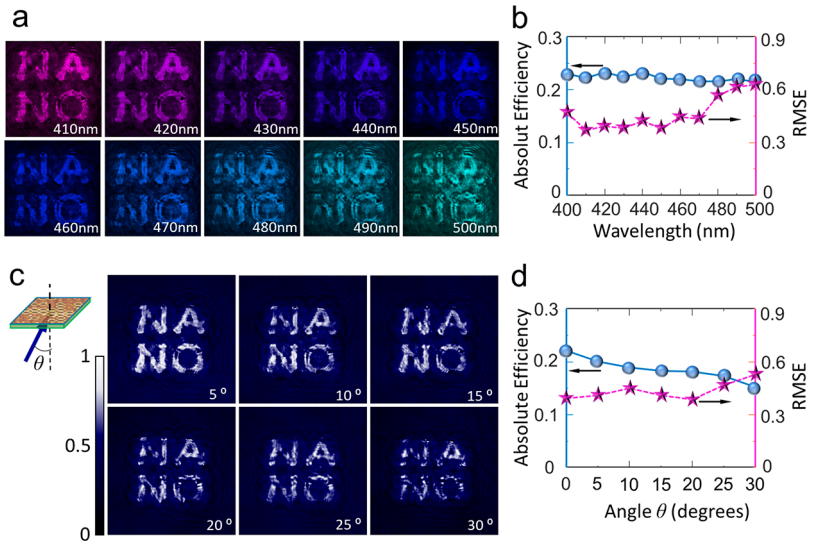

Figure 3. Broadband and large angle-of-view features of the MoS_2 photon nanosieve hologram. (a) Measured holographic images at different wavelengths. (b) Experimental absolute efficiency (solid circle) and RMSE (star) at the wavelengths from 400 to 500 nm. The RMSE is calculated by using the measured and ideal holographic images. (c) Measured holographic image under the oblique illumination from 5 to 30°. The inset shows the sketch of experimental measurement. (d) Experimental absolute efficiency (solid circle) and RMSE (star) under the different incident angle.

plane permittivity has a trivial influence on the optical response[22,33] and is therefore ignored. Using a 10 nm thick MoS_2 film, our FDTD simulations (Figure 1e) unveil that a 220 nm diameter hole is well-defined optically by confining an electric dipole-like mode within the circular hole, blocking the transmission of light outside the hole.

■ MOS_2-BASED NANOHOLOGRAMS

Figure 2a, b shows the designed holograms (see the Supporting Information) based on random MoS_2 photon sieves and the simulated holographic image at the target plane, respectively. With the processes (Supporting Information) illustrated in Figure 2c, all the devices in this work are fabricated by using focused-ion-beam (FIB) lithography. The scanning-electron-microscope (SEM) image (Figure 2d) of FIB-patterned photon nanosieves with gold film indicates high-fidelity holes with clear contours. To evaluate the lateral dimension, we extract the line-scanning gray scale value (Figure 2e) from its SEM image, showing the expected diameter of ~220 nm. The minor thickness of the film enables a shorter etching time, such that the side wall of holes is less influenced by scattering ions. This helps us to reliably etch neighboring nanoholes with an edge-to-edge distance of only 30 nm. The morphology (Figure 2f) of the MoS_2 photon sieves, as mapped by the atomic force microscope (AFM), unveils a 4 nm thickness between the surface of MoS_2 film and the bottom of the etched holes (Figure 2g). Our experiment confirms that no Raman signal is observed at the etched location of the sample (Figure S3), indicating that the MoS_2 within the hole is removed completely. It implies that the 10 nm thickness of the original MoS_2 film is reduced to 4 nm (doubly confirmed by the Raman shift of 25 cm^{-1} (relative to five- or six-layer MoS_2) in Figure S3, and the agreement between the experimental and simulated transmission in Figure S4) during our process. The hole diameter in the AFM image is slightly smaller than 220 nm, which is caused by the resolution of the AFM tip (30 nm in radius).

By using a self-built setup, we measure the experimental holographic image (Figure 2h), which has good agreement with the simulation (Figure 2b). The image quality is evaluated by using the root-mean-square error (RMSE) between the ideal and holographic images, which are calculated as 15.5% (simulation) and 38.0% (experiment). The discrepancy originates mainly from the undesired background through the MoS_2 film.

To measure its efficiency, we record the power of incident light and holographic image by using a camera (Figure S5). Calculated by the ratio of the power of holographic image to the total power incident on the hologram, the experimental absolute efficiency (Section 6 in the Supporting Information) is ~22%, which is ~11 times that of the metallic photon-sieve holograms.[23] Because of the transmission through the film, the resulting efficiency contains three parts: (1) the holographic image contributed by only the nanoholes, (2) the diffraction pattern created by only the film transmission, and (3) the coherent interaction between holographic image and the diffraction pattern of film transmission (see Figure S6 and Section 7 in the Supporting Information). The last two parts lead to the efficiency enhancement of "NANO" image but reduce the contrast of image due to the increased background. Moreover, compared with the 2D material meta-devices[10−14] with the thickness from a few to tens of nanometers, our 2D material hologram shows the record-high efficiency.

Figure 3a shows the pseudocolor profiles of captured images over a wide spectrum. The background of experimental images is trivial at short wavelengths (410−450 nm), whereas it increases at the long-wavelength spectrum, as confirmed by the experimental RMSEs (Figure 3b) between the measured and ideal images. The measured efficiency (Figure 3b) shows a constant of ~20% over the spectrum of interest. Such a counterintuitive result is mainly caused by the fact that the deep-subwavelength thickness of film holds over this spectral range, so that the transmission of light passing through the holes is seldom affected by the illuminating wavelength. The nearly constant efficiency in our MoS_2-based hologram is

https://dx.doi.org/10.1021/acs.nanolett.0c02712
Nano Lett. 2020, 20, 7964−7972

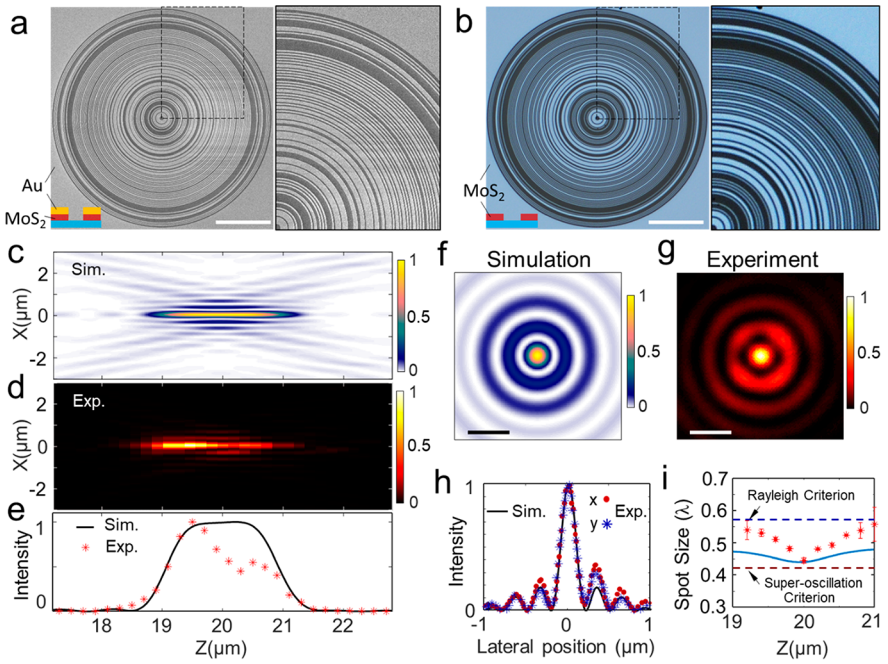

Figure 4. MoS_2-based supercritical lens. (a) SEM and (b) microscopic images of fabricated lens before and after removing the top gold layer. Scale bars: 20 μm. (c) Simulated and (d) experimental intensity profiles at the $x-z$ plane. In d, the measured needle is not well-mapped because of the slight deviation of optical axis during the z-direction scanning. So, we provide the $x-z$ intensity profiles around the focal plane, which is extracted from the $x-y$ intensity profiles at different z-cut planes from z = 19 μm to z = 21 μm. (e) Comparison of on-axis intensity between simulation and experiment. (f) Simulated and (g) measured spot at the focal plane. Scale bars: 500 nm. (h) Simulated and experimental line-scanning intensity profiles. The x- and y-scanning profiles in measured spot are shown by red dots and blue stars, respectively. (i) Spot size of optical needle from z = 19 μm to z = 21 μm. The Rayleigh and superoscillation criteria are given, respectively, by 0.515λ/NA (FWHM) and 0.38λ/NA. The experimental results (labeled by red stars) showed subdiffraction focusing below Rayleigh criterion. The blue curve is simulated focusing spot size.

unique compared with traditional holograms,[38] metasurface holograms,[39] and other nanometer-thick holograms,[40] where the efficiency depends strongly on the wavelength.

The angle of view is experimentally characterized by tuning the incident angle θ (Figure 3c) at the exemplified wavelength of 450 nm. The contour and uniformity of holographic images get worse as the angle θ increases. However, the distinguishable image at θ = 30° implies a larger angle-of-view of 60° × 60° compared with metal-based holograms.[26] In Figure 3d, the efficiency of hologram reduces to ~15% efficiency at an angle of θ = 30°, which represents a lower decreasing rate of efficiency than those of dielectric metasurfaces.[41] The transmission of our 2D material hologram is less affected by the oblique incidence, because the nanometer thickness of hole significantly decreases the coupling length between light and holes. In comparison, the dielectric metasurfaces realize high efficiency with optically induced electromagnetic modes. These modes can be excited by only the transverse components of incident field, where the efficiency decreases dramatically under the tilting incidence.[41] The additional tilting phase destroys the uniformity of holographic images and thus leads to the increased RMSEs (Figure 3d).

■ MoS_2-BASED SUPERCRITICAL LENS

We also demonstrate a MoS_2-based flat lens that could realize the focusing beyond Rayleigh diffraction limit. Although the superoscillation phenomenon,[23,30,42,43] known as the fact that a band-limited function can oscillate locally faster than its largest Fourier component, could be used to create an arbitrarily small hotspot, the accompanying strong sidelobe constrains the field-of-view in imaging. Therefore, we design a supercritical lens (SCL) that generates an optical needle with the lateral size slightly larger than the superoscillation (SOL) criterion of 0.38λ/NA (NA is the numerical aperture of a lens).[24,25,44] Such a SCL usually has a well-confined hotspot without any significant sideband for the easier usage in practical applications. The designed SCL with 46 concentric transparent belts (Table S1) has an NA of ~0.9 with a diameter of 80 μm and a focal length of 20 μm.

Figure 4a, b presents the SEM image of the gold-MoS_2 sample and the microscopy image of the final pure-MoS_2 lens, respectively. To characterize the needlelike field, we first measure the diffraction pattern after the lens. Figure 4c, d show the simulated and measured intensity profiles at the $x-z$ plane, where the focused light is collected experimentally by an NA = 0.9 objective lens and then projected onto a camera. Both on-axis intensity profiles are shown in Figure 4e, where the inhomogeneous experimental needle originates from the imperfect wavefront of incident light (Figure S7). The focal spot with the lateral size of ~0.44λ (~198 nm, evaluated by the full width at half-maximum (FWHM)), is achieved at λ = 450 nm in simulation (Figure 4f) and experiment (Figure 4g). Their line-scanning intensity profiles agree well (Figure 4h), thus verifying the superfocusing beyond Rayleigh diffraction limit of 257.5 nm (0.515λ/NA by FWHM). Superior to other lenses with atom-level thickness, our MoS_2 lens is able to produce the subwavelength hotspot and break diffraction limit over a long propagating distance of ~2 μm (Figure 4i). Such a depth-of-focus of 5λ makes the proposed 2D SCL suitable for imaging and lithography.

https://dx.doi.org/10.1021/acs.nanolett.0c02712
Nano Lett. 2020, 20, 7964−7972

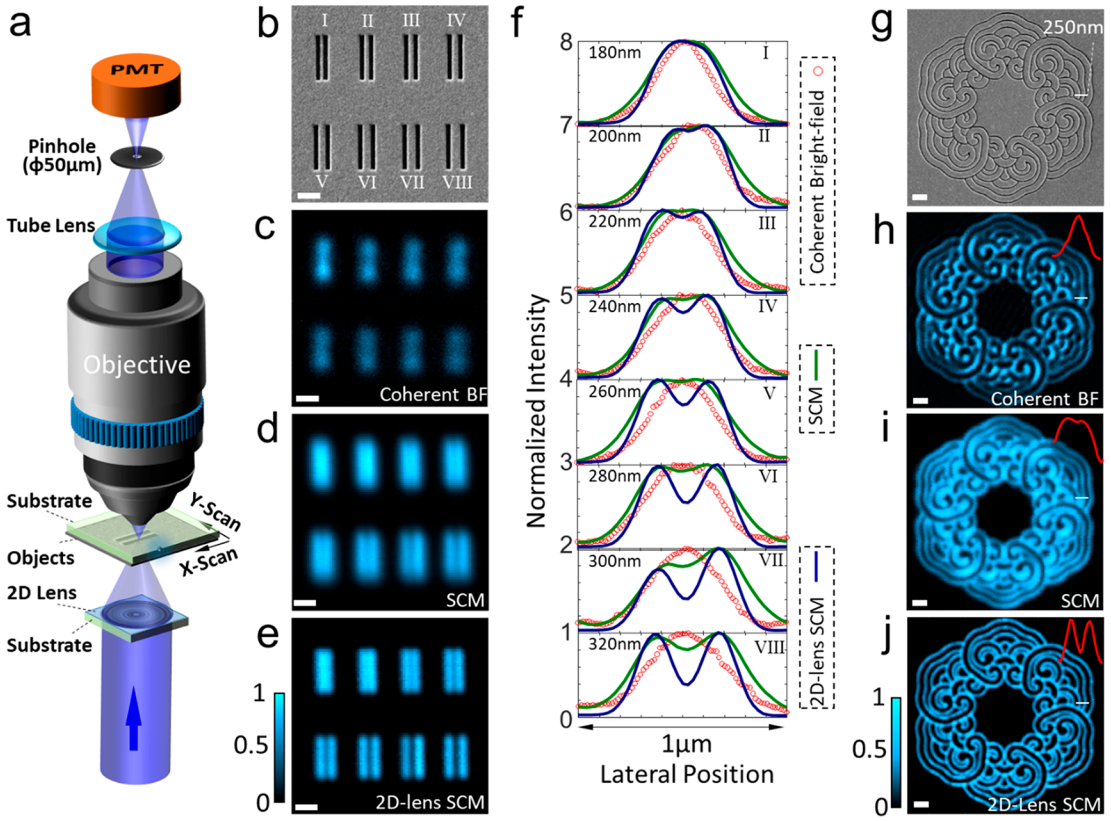

Figure 5. Nanoimaging by 2D SCL microscopy. (a) Sketch of 2D SCL scanning confocal microscopy. (b–e) Images of double slits taken by (b) SEM, (c) bright-field (BF) microscopy, (d) traditional scanning confocal microscopy (SCM), and (e) our 2D lens SCM. In b, the widths of slits are 110 nm, and their center-to-center distances are 180 nm (I), 200 nm (II), 220 nm (III), 240 nm (IV), 260 nm (V), 280 nm (VI), 300 nm (VII), and 320 nm (VIII), respectively. Scale bars: 500 nm. (f) Line-scanning intensity profiles of the experimentally captured images by addressing the center-to-center distances from 180 to 320 nm at an interval of 20 nm. The resolvable CTC distances are 240 nm for traditional SCM and 200 nm for our 2D lens SCM. The coherent BF microscopy cannot resolve any double slit used in this work. (g–j) Images of a complex object (an auspicious cloud totem) captured by (g) SEM, (h) bright-field microscopy, (i) traditional SCM and (j) our 2D lens SCM. The insets in h, i, and j show the line-scanning intensity along the white line. Scale bars: 1 μm.

Table 1. Comparison among Flat-Lens-Based Scanning Confocal Microscopies

	material	thickness (nm)	wavelength, λ (nm)	ambient medium	feature size of objects	gap resolution	center-to-center resolution
Rogers et al.[42]	Al	100	640	oil	210	105 nm (0.164λ)	315 nm (0.492λ)
Qin et al.[25]	Cr	100	405	air	163	65 nm (0.161λ)	228 nm (0.563λ)
Chen et al.[45]	TiO_2	600	532	water	200	200 nm (0.376λ)	400 nm (0.752λ)
This work	MoS_2	10	450	air	110	90 nm (0.2λ)	200 nm (0.444λ)

HIGH-QUALITY NANOIMAGING

We integrate this MoS_2-based 2D SCL into a scanning confocal microscopy (SCM) for high-quality imaging application. The working principle is sketched in Figure 5a and discussed in the Supporting Information. To test its resolution, we investigate the imaging results for various objects that are made in an opaque film. Figure 5b shows the SEM image of 110 nm-wide double slits with the center-to-center (CTC) distances ranging from 180 to 320 nm. As a control experiment, the coherent bright-field (BF) microscopy with a 0.9 NA objective lens is used under the illumination of a 450 nm wavelength laser, for a fair comparison. However, it fails to resolve all these slits (Figure 5c) because of the coherent superposition of the point spread function. Consequently, the coherent BF microscopy (see experiment in Figure 5c and simulation in Figure S8) usually behaves worse than the incoherent BF microscopy (see experiment in Figure S9 and simulation in Figure S10) with the imaging resolution of 0.61λ/NA. The traditional SCM, employing a 0.9 NA objective lens as the condenser to focus a coherent 450 nm laser, demonstrates the imaging resolution of ~240 nm (Figure 5d). In comparison, the images taken by our 2D SCL SCM are displayed in Figure 5e, where the slits with the CTC distance of 200 nm can be distinguished clearly with a valley of intensity. In Figure 5f, a quantitative comparison between their line-scanning intensity profiles doubly confirms that our 2D SCL microscopy has the CTC resolution of 200 nm (i.e., 0.44λ at λ = 450 nm), which coincides with the spot size of 198 nm. Considering the width (i.e., 110 nm) of slits, a gap of 90 nm is resolved by using our 2D SCL microscopy. The CTC resolution is improved in comparison with the previously reported CTC resolutions of 0.492λ (λ = 640 nm),[42] 0.563λ (λ = 405 nm)[25] and 0.752λ (λ = 532 nm)[45] (see Table 1). Theoretically, the point-spread function of a coherent SCM can be described by $h = |h_1 h_2|^2$,[46] where h_1 and h_2 are the pulse response of the condenser and the collection objective,

https://dx.doi.org/10.1021/acs.nanolett.0c02712
Nano Lett. 2020, 20, 7964–7972

respectively. By decreasing the size of h_1, the 2D lens and other flat-lens SCMs[25,42] could resolve the finer details of objects better than the metalens-based SCM[45] with a diffraction-limit h_1.

Furthermore, we carry out the imaging of a more complex object containing the curved 50 nm width slits (Figure 5g). Labeled by the white lines in Figure 5g–j, the CTC distance between two neighboring slits is around 250 nm, which cannot be resolved by the coherent bright-field microscopy (Figure 5h). Although the SCM can resolve these two slits (Figure 5i), such a scale approaches its resolving power due to the small valley of intensity. In Figure 5j, our MoS_2-based 2D SCL microscopy shows the clear image with the fine details, where the imaged curves have different orientations but keep the identical width. It implies that the imaging resolution is homogeneous across the entire $x-y$ plane. Therefore, the scanning mode enables our 2D SCL SCM to exclude optical aberrations such as coma and distortion, achieving a well-behaved image of 10 μm × 10 μm.

DISCUSSION

As illustrated in Table 1, our 2D SCL microscopy has superior properties including ultrasmall thickness, record-small feature of objects, and high resolution compared with other reported SCMs.[25,42,45] Although the resolved gap of 0.2λ in this work is slightly larger than ∼0.16λ in previous reports,[25,42] it could be improved by increasing the feature size of objects. For our microscopy, the CTC resolution mainly depends on the spot size of a lens, which could be suppressed further by using a larger-*NA* lens immersed in liquid or solid. Furthermore, our simulations (Figures S8–S10) suggest that the incoherent illumination could improve the imaging resolution further, but the problem of decreasing a focal spot for the noncoherent light arises.

The proposed photon sieves have large regions that have not been patterned. If these regions are filled with other shaped holes, these devices will gain more transmission and efficiency by introducing the amplitude and phase modulation simultaneously. The thin film facilitates the fabrication of high-precision nanostructures, as observed from the edge-to-edge distance of 30 nm. Such a big advantage is critical especially when we move to deep ultraviolet range where only the amplitude photon sieves work due to the lack of other compatible materials. Note that TMDCs have been experimentally verified with the giant tenability of refractive index (both the real and imaginary parts) at the visible-wavelength range by using complementary metal–oxide–semiconductor compatible electrical grating.[47] This important property enables our TMDCs-based meta-optics with electrical tunability[48] for dynamic wavefront shaping.

CONCLUSION

In summary, we propose a high-quality optical platform using atomically thin TMDC layers by utilizing high exciton absorption due to the band-nesting effect. Through fabricating well-designed nanostructures on the MoS_2 film, we show 2D photon nanosieves and 2D supercritical lens with the thickness shrunk to just ∼10 nm. Large angle-of-view hologram with greatly enhanced efficiency and high-performance scanning imaging with a resolution of 0.44λ is demonstrated. Our work enriches the fundamental physics of modulating optical amplitude via 2D TMDCs for next-generation nanometer optics in holography, imaging, and metrology.

ASSOCIATED CONTENT

Supporting Information

The Supporting Information is available free of charge at https://pubs.acs.org/doi/10.1021/acs.nanolett.0c02712.

Growth of MoS_2 layers; fabrication; hologram design; experimental setup; efficiency measurement; lens design; 2D SCL scanning confocal microscopy; absorbance spectra of PVD-grown MoS2 samples; sketches of measuring the total efficiency of the 2D nanosieve hologram; simulated SCL intensity profiles at the $x-z$ plane; background effects caused by transmitted light from the unpatterned film in hologram; a comparison between the simulated and experimental results for these microscopies (BF, SCM, and 2D lens SCM) under coherent illumination; imaging results by using incoherent bright-field microscopy; a comparison between the simulated and experimental results for these microscopies (BF, SCM, and 2D lens SCM) under incoherent conditions; size effect of pinhole in a traditional incoherent scanning confocal microscopy; dimension of designed SCL (PDF)

AUTHOR INFORMATION

Corresponding Authors

Kun Huang – *Department of Optics and Optical Engineering, University of Science and Technology of China, Hefei, Anhui 230026, China;* orcid.org/0000-0002-9391-149X; Email: huangk17@ustc.edu.cn

Jinghua Teng – *Institute of Materials Research and Engineering, Agency for Science, Technology and Research (A*STAR), Singapore 138634 Singapore;* orcid.org/0000-0001-5331-3092; Email: jh-teng@imre.a-star.edu.sg

Authors

Zeng Wang – *Institute of Materials Research and Engineering, Agency for Science, Technology and Research (A*STAR), Singapore 138634 Singapore;* orcid.org/0000-0002-0730-8601

Guanghui Yuan – *Centre for Disruptive Photonic Technologies, The Photonic Institute, SPMS, Nanyang Technological University, Singapore 637371 Singapore;* orcid.org/0000-0002-4585-9711

Ming Yang – *Institute of Materials Research and Engineering, Agency for Science, Technology and Research (A*STAR), Singapore 138634 Singapore;* orcid.org/0000-0002-0876-1221

Jianwei Chai – *Institute of Materials Research and Engineering, Agency for Science, Technology and Research (A*STAR), Singapore 138634 Singapore*

Qing Yang Steve Wu – *Institute of Materials Research and Engineering, Agency for Science, Technology and Research (A*STAR), Singapore 138634 Singapore;* orcid.org/0000-0003-2525-8334

Tao Wang – *Institute of Materials Research and Engineering, Agency for Science, Technology and Research (A*STAR), Singapore 138634 Singapore*

Matej Sebek – *Institute of Materials Research and Engineering, Agency for Science, Technology and Research (A*STAR), Singapore 138634 Singapore; Department of Physics and*

Astronomy, University College London, London WC1E 6BT, United Kingdom

Dan Wang − *State Key Laboratory of integrated optoelectronics, College of Electronic Science and Engineering, Jilin University, Changchun, Jilin 130012, China*

Lei Wang − *State Key Laboratory of integrated optoelectronics, College of Electronic Science and Engineering, Jilin University, Changchun, Jilin 130012, China*

Shijie Wang − *Institute of Materials Research and Engineering, Agency for Science, Technology and Research (A*STAR), Singapore 138634 Singapore*

Dongzhi Chi − *Institute of Materials Research and Engineering, Agency for Science, Technology and Research (A*STAR), Singapore 138634 Singapore;* orcid.org/0000-0001-9562-1595

Giorgio Adamo − *Centre for Disruptive Photonic Technologies, The Photonic Institute, SPMS, Nanyang Technological University, Singapore 637371 Singapore;* orcid.org/0000-0003-1974-3368

Cesare Soci − *Centre for Disruptive Photonic Technologies, The Photonic Institute, SPMS, Nanyang Technological University, Singapore 637371 Singapore;* orcid.org/0000-0002-0149-9128

Handong Sun − *Centre for Disruptive Photonic Technologies, The Photonic Institute, SPMS and Division of Physics and Applied Physics, School of Physical and Mathematical Sciences, Nanyang Technological University, Singapore 637371 Singapore;* orcid.org/0000-0002-2261-7103

Complete contact information is available at: https://pubs.acs.org/10.1021/acs.nanolett.0c02712

Author Contributions

†Z.W. and G.Y. contributed equally to this work.

Author Contributions

K.H. and J.T. conceived the idea. K.H. performed the numerical simulations and designed the holograms. G.Y. carried out the lens design. Z.W. fabricated the sample. M.Y., J.C., Z.W., Q.Y., W.S., M.S., and S.W. grew and characterized the multilayered MoS2. T.W. characterized the AFM images. D.W. and L.W. contributed to the MoS2 band structure calculation. Z.W. and G.Y. implemented the measurement. K.H., Z.W., G.Y., and J.T. wrote the manuscript. J.T., K.H., C.S., H.S., and G.A. supervised the overall project. All authors discussed the results, did the data analysis, and commented on the manuscript.

Notes

The authors declare no competing financial interest.

■ ACKNOWLEDGMENTS

The work is financially supported by the Agency for Science, Technology and Research (A*STAR) Singapore under Grants 152700014 and 152700012. K.H. thanks CAS Pioneer Hundred Talents Program, "the Fundamental Research Funds for the Central Universities" in China, USTC Research Funds of the Double First-Class Initiative (Grant YD2030002003), the National Natural Science Foundation of China (Grant 61875181 and 61705085), and the support from the University of Science and Technology of China's Centre for Micro and Nanoscale Research and Fabrication. G.Y., G.A., and C.S. acknowledge the support from the Agency for Science, Technology and Research (A*STAR) Singapore (Grant SERC A1685b0005) and Singapore Ministry of Education Academic Research Fund Tier 3 (MOE2016-T3-1-006 (S)). H.S. acknowledges the support from the Singapore Ministry of Education through the Academic Research Fund under Project Tier 1-RG189/17(S). We thank Prof. Nikolay Zheludev for the valuable discussions. Z.W. thanks the support from Ms. Zhang Xin and Dr. Zhao Rui.

■ REFERENCES

(1) Goodman, J. W. *Introduction to Fourier Optics*; Roberts and Company Publishers: Englewood, CO, 2005.

(2) Yu, N.; Genevet, P.; Kats, M. A.; Aieta, F.; Tetienne, J.-P.; Capasso, F.; Gaburro, Z. Light propagation with phase discontinuities: generalized laws of reflection and refraction. *Science* **2011**, *334* (6054), 333−337.

(3) Zhang, L.; Mei, S.; Huang, K.; Qiu, C.-W. Advances in Full Control of Electromagnetic Waves with Metasurfaces. *Adv. Opt. Mater.* **2016**, *4* (6), 818−833.

(4) Huang, K.; Zhao, D.; Tjiptoharsono, F.; Chen, Y.; Wong, C. P. Y.; Tang, X.; Yang, J. K. W.; Dong, Z. Bio-inspired Photonic Masquerade with Perturbative Metasurfaces. *ACS Nano* **2020**, *14* (6), 7529−7537.

(5) Pu, M.; Li, X.; Ma, X.; Wang, Y.; Zhao, Z.; Wang, C.; Hu, C.; Gao, P.; Huang, C.; Ren, H.; Li, X.; Qin, F.; Yang, J.; Gu, M.; Hong, M.; Luo, X. Catenary optics for achromatic generation of perfect optical angular momentum. *Sci. Adv.* **2015**, *1* (9), No. e1500396.

(6) Zhang, F.; Pu, M.; Li, X.; Gao, P.; Ma, X.; Luo, J.; Yu, H.; Luo, X. All-Dielectric Metasurfaces for Simultaneous Giant Circular Asymmetric Transmission and Wavefront Shaping Based on Asymmetric Photonic Spin-Orbit Interactions. *Adv. Funct. Mater.* **2017**, *27* (47), 1704295.

(7) Guo, Y.; Ma, X.; Pu, M.; Li, X.; Zhao, Z.; Luo, X. High-efficiency and wide-angle beam steering based on catenary optical fields in ultrathin metalens. *Adv. Opt. Mater.* **2018**, *6* (19), 1800592.

(8) Jackson, J. D. *Classical Electrodynamics*; Wiley: New York, 1999.

(9) Manzeli, S.; Ovchinnikov, D.; Pasquier, D.; Yazyev, O. V.; Kis, A. 2D transition metal dichalcogenides. *Nat. Rev. Mater.* **2017**, *2*, 17033.

(10) Kong, X.-T.; Khan, A. A.; Kidambi, P. R.; Deng, S.; Yetisen, A. K.; Dlubak, B.; Hiralal, P.; Montelongo, Y.; Bowen, J.; Xavier, S. p.; et al. Graphene-based ultrathin flat lenses. *ACS Photonics* **2015**, *2* (2), 200−207.

(11) Yang, J.; Wang, Z.; Wang, F.; Xu, R.; Tao, J.; Zhang, S.; Qin, Q.; Luther-Davies, B.; Jagadish, C.; Yu, Z.; Lu, Y. Atomically thin optical lenses and gratings. *Light: Sci. Appl.* **2016**, *5* (3), No. e16046.

(12) Wang, Y.; Deng, Z.-L.; Hu, D.; Yuan, J.; Ou, Q.; Qin, F.; Zhang, Y.; Ouyang, X.; Li, Y.; Peng, B.; Cao, Y.; Guan, B.; Zhang, Y.; He, J.; Qiu, C.-W.; Bao, Q.; Li, X. Atomically Thin Noble Metal Dichalcogenides for Phase-Regulated Meta-optics. *Nano Lett.* **2020**, DOI: 10.1021/acs.nanolett.0c01805.

(13) Yue, Z.; Xue, G.; Liu, J.; Wang, Y.; Gu, M. Nanometric holograms based on a topological insulator material. *Nat. Commun.* **2017**, *8*, 15354.

(14) Lin, H.; Xu, Z.-Q.; Cao, G.; Zhang, Y.; Zhou, J.; Wang, Z.; Wan, Z.; Liu, Z.; Loh, K. P.; Qiu, C.-W.; Bao, Q.; Jia, B. Diffraction-limited imaging with monolayer 2D material-based ultrathin flat lenses. *Light: Sci. Appl.* **2020**, *9* (1), 137.

(15) Liu, C.-H.; Zheng, J.; Colburn, S.; Fryett, T. K.; Chen, Y.; Xu, X.; Majumdar, A. Ultrathin van der Waals Metalenses. *Nano Lett.* **2018**, *18*, 6961−6966.

(16) Zheng, X.; Jia, B.; Lin, H.; Qiu, L.; Li, D.; Gu, M. Highly efficient and ultra-broadband graphene oxide ultrathin lenses with three-dimensional subwavelength focusing. *Nat. Commun.* **2015**, *6*, 8433.

(17) Hu, G.; Hong, X.; Wang, K.; Wu, J.; Xu, H.-X.; Zhao, W.; Liu, W.; Zhang, S.; Garcia-Vidal, F.; Wang, B.; Lu, P.; Qiu, C.-W. Coherent steering of nonlinear chiral valley photons with a synthetic Au-WS2 metasurface. *Nat. Photonics* **2019**, *13*, 467−472.

(18) Dasgupta, A.; Gao, J.; Yang, X. Atomically Thin Nonlinear Transition Metal Dichalcogenide Holograms. *Nano Lett.* **2019**, *19* (9), 6511−6516.
(19) Carvalho, A.; Ribeiro, R. M.; Castro Neto, A. H. Band nesting and the optical response of two-dimensional semiconducting transition metal dichalcogenides. *Phys. Rev. B: Condens. Matter Mater. Phys.* **2013**, *88* (11), 115205.
(20) Yim, C.; O'Brien, M.; McEvoy, N.; Winters, S.; Mirza, I.; Lunney, J. G.; Duesberg, G. S. Investigation of the optical properties of MoS2 thin films using spectroscopic ellipsometry. *Appl. Phys. Lett.* **2014**, *104* (10), 103114.
(21) Wang, L.; Wang, Z.; Wang, H.-Y.; Grinblat, G.; Huang, Y.-L.; Wang, D.; Ye, X.-H.; Li, X.-B.; Bao, Q.; Wee, A.-S.; Maier, S. A.; Chen, Q.-D.; Zhong, M.-L.; Qiu, C.-W.; Sun, H.-B. Slow cooling and efficient extraction of C-exciton hot carriers in MoS2 monolayer. *Nat. Commun.* **2017**, *8*, 13906.
(22) Verre, R.; Baranov, D. G.; Munkhbat, B.; Cuadra, J.; Käll, M.; Shegai, T. Transition metal dichalcogenide nanodisks as high-index dielectric Mie nanoresonators. *Nat. Nanotechnol.* **2019**, *14*, 679−683.
(23) Huang, K.; Liu, H.; Garcia-Vidal, F. J.; Hong, M.; Luk'yanchuk, B.; Teng, J.; Qiu, C.-W. Ultrahigh-capacity non-periodic photon sieves operating in visible light. *Nat. Commun.* **2015**, *6*, 7059.
(24) Huang, K.; Qin, F.; Liu, H.; Ye, H.; Qiu, C.-W.; Hong, M.; Luk'yanchuk, B.; Teng, J. Planar Diffractive Lenses: Fundamentals, Functionalities, and Applications. *Adv. Mater.* **2018**, *30* (0), 1704556.
(25) Qin, F.; Huang, K.; Wu, J.; Teng, J.; Qiu, C.-W.; Hong, M. A Supercritical Lens Optical Label-Free Microscopy: Sub-Diffraction Resolution and Ultra-Long Working Distance. *Adv. Mater.* **2017**, *29*, 1602721.
(26) Huang, K.; Liu, H.; Si, G.; Wang, Q.; Lin, J.; Teng, J. Photon-nanosieve for ultrabroadband and large-angle-of-view holograms. *Laser Photonics Rev.* **2017**, *11*, 1700025.
(27) Park, J.; Lee, K.; Park, Y. Ultrathin wide-angle large-area digital 3D holographic display using a non-periodic photon sieve. *Nat. Commun.* **2019**, *10* (1), 1304.
(28) Mei, S.; Mehmood, M. Q.; Hussain, S.; Huang, K.; Ling, X.; Siew, S. Y.; Liu, H.; Teng, J.; Danner, A.; Qiu, C.-W. Flat Helical Nanosieves. *Adv. Funct. Mater.* **2016**, *26*, 5255−5262.
(29) Mehmood, M.; Mei, S.; Hussain, S.; Huang, K.; Siew, S.; Zhang, L.; Zhang, T.; Ling, X.; Liu, H.; Teng, J.; et al. Visible-Frequency Metasurface for Structuring and Spatially Multiplexing Optical Vortices. *Adv. Mater.* **2016**, *28* (13), 2533−2539.
(30) Yuan, G. H.; Zheludev, N. I. Detecting nanometric displacements with optical ruler metrology. *Science* **2019**, *364*, 771−775.
(31) Roberts, A. Electromagnetic Theory of Diffraction by a Circular Aperture in a Thick, Perfectly Conducting Screen. *J. Opt. Soc. Am. A* **1987**, *4* (10), 1970−1983.
(32) Onida, G.; Reining, L.; Rubio, A. Electronic excitations: density-functional versus many-body Green's-function approaches. *Rev. Mod. Phys.* **2002**, *74* (2), 601.
(33) Yu, Y.; Yu, Y.; Cai, Y.; Li, W.; Gurarslan, A.; Peelaers, H.; Aspnes, D. E.; Van de Walle, C. G.; Nguyen, N. V.; Zhang, Y.-W.; Cao, L. Exciton-dominated dielectric function of atomically thin MoS 2 films. *Sci. Rep.* **2015**, *5*, 16996.
(34) Palik, E. D. *Handbook of Optical Constants of Solids*; Academic Press, 1998.
(35) Weber, J.; Calado, V.; Van De Sanden, M. Optical constants of graphene measured by spectroscopic ellipsometry. *Appl. Phys. Lett.* **2010**, *97* (9), 091904.
(36) Taguchi, A.; Hayazawa, N.; Furusawa, K.; Ishitobi, H.; Kawata, S. Deep-UV tip-enhanced Raman scattering. *J. Raman Spectrosc.* **2009**, *40* (9), 1324−1330.
(37) Lozanova, V.; Lalova, A.; Soserov, L.; Todorov, R. Optical and electrical properties of very thin chromium films for optoelectronic devices. *J. Phys.: Conf. Ser.* **2014**, *514*, 012003.
(38) Huang, K.; Gao, H. F.; Cao, G. W.; Shi, P.; Zhang, X. B.; Li, Y. Design of DPE for modulating the electric field at the out-of-focus plane in a lens system. *Appl. Opt.* **2012**, *51* (21), 5149−5153.
(39) Huang, K.; Dong, Z.; Mei, S.; Zhang, L.; Liu, Y.; Liu, H.; Zhu, H.; Teng, J.; Luk'yanchuk, B.; Yang, J. K.; Qiu, C. Silicon multi-meta-holograms for the broadband visible light. *Laser Photonics Rev.* **2016**, *10* (3), 500−509.
(40) Wang, H. C.; Chu, C. H.; Wu, P. C.; Hsiao, H. H.; Wu, H. J.; Chen, J. W.; Lee, W. H.; Lai, Y. C.; Huang, Y. W.; Tseng, M. L.; et al. Ultrathin Planar Cavity Metasurfaces. *Small* **2018**, *14* (17), 1703920.
(41) Huang, K.; Deng, J.; Leong, H. S.; Yap, S. L. K.; Yang, R. B.; Teng, J.; Liu, H. Ultraviolet Metasurfaces of ≻80% Efficiency with Antiferromagnetic Resonances for Optical Vectorial Anti-Counterfeiting. *Laser Photonics Rev.* **2019**, *13* (5), 1800289.
(42) Rogers, E. T.; Lindberg, J.; Roy, T.; Savo, S.; Chad, J. E.; Dennis, M. R.; Zheludev, N. I. A super-oscillatory lens optical microscope for subwavelength imaging. *Nat. Mater.* **2012**, *11* (5), 432−435.
(43) Tang, D.; Wang, C.; Zhao, Z.; Wang, Y.; Pu, M.; Li, X.; Gao, P.; Luo, X. Ultrabroadband superoscillatory lens composed by plasmonic metasurfaces for subdiffraction light focusing. *Laser Photonics Rev.* **2015**, *9*, 713.
(44) Huang, K.; Ye, H.; Teng, J.; Yeo, S. P.; Luk'yanchuk, B.; Qiu, C. W. Optimization-free superoscillatory lens using phase and amplitude masks. *Laser Photonics Rev.* **2014**, *8* (1), 152−157.
(45) Chen, W. T.; Zhu, A. Y.; Khorasaninejad, M.; Shi, Z.; Sanjeev, V.; Capasso, F. Immersion Meta-Lenses at Visible Wavelengths for Nanoscale Imaging. *Nano Lett.* **2017**, *17* (5), 3188−3194.
(46) Wilson, T.; Sheppard, C. *Theory and Practice of Scanning Optical Microscopy*; Academic Press, London, 1984; Vol. *180*.
(47) Yu, Y.; Yu, Y.; Huang, L.; Peng, H.; Xiong, L.; Cao, L. Giant gating tunability of optical refractive index in transition metal dichalcogenide monolayers. *Nano Lett.* **2017**, *17* (6), 3613−3618.
(48) van de Groep, J.; Song, J.-H.; Celano, U.; Li, Q.; Kik, P. G.; Brongersma, M. L. Exciton resonance tuning of an atomically thin lens. *Nat. Photonics* **2020**, *14*, 426−430.
(49) Toyozawa, Y. Theory of line-shapes of the exciton absorption bands. *Prog. Theor. Phys.* **1958**, *20* (1), 53−81.
(50) Wang, H.; Xie, W.; Wang, Y.; Zhu, J.; Liu, M.; Lu, W.; Deng, Y.; Wang, G.; Wang, D. Fabrication of 3D nanovolcano-shaped nanopores with helium ion microscopy. *J. Vac. Sci. Technol., B: Nanotechnol. Microelectron.: Mater., Process., Meas., Phenom.* **2018**, *36* (1), 011603.

https://dx.doi.org/10.1021/acs.nanolett.0c02712
Nano Lett. 2020, 20, 7964−7972